Functional connectivity modeling of consistent cortico-striatal degeneration in Huntington's disease

Imis Dogan[a,b,c], Claudia R. Eickhoff[b,d], Peter T. Fox[e], Angela R. Laird[f], Jörg B. Schulz[a,c], Simon B. Eickhoff[b,g,1], Kathrin Reetz[a,b,c,1,*]

[a]Department of Neurology, RWTH Aachen University, Pauwelsstr. 30, 52074 Aachen, Germany
[b]Institute of Neuroscience and Medicine (INM-1, INM-4), Research Center Jülich GmbH, 52425 Jülich, Germany
[c]JARA — Translational Brain Medicine, Aachen, Jülich, Germany
[d]Department of Psychiatry, Psychotherapy and Psychosomatic, RWTH Aachen University, Pauwelsstr. 30, 52074 Aachen, Germany
[e]Research Imaging Center, University of Texas Health Science Center, 7703 Floyd Curl Drive, San Antonio, TX 78284-7801, USA
[f]Department of Physics, Florida International University, Modesto A. Maidique Campus, CP 204, 11200 SW 8th Street, Miami, FL 33199, USA
[g]Institute of Clinical Neuroscience and Medical Psychology, Heinrich-Heine University, Universitätsstr. 1, 40225 Düsseldorf, Germany

ARTICLE INFO

ABSTRACT

Huntington's disease (HD) is a progressive neurodegenerative disorder characterized by a complex neuropsychiatric phenotype. In a recent meta-analysis we identified core regions of consistent neurodegeneration in premanifest HD in the striatum and middle occipital gyrus (MOG). For early manifest HD convergent evidence of atrophy was most prominent in the striatum, motor cortex (M1) and inferior frontal junction (IFJ). The aim of the present study was to functionally characterize this topography of brain atrophy and to investigate differential connectivity patterns formed by consistent cortico-striatal atrophy regions in HD. Using areas of striatal and cortical atrophy at different disease stages as seeds, we performed task-free resting-state and task-based meta-analytic connectivity modeling (MACM). MACM utilizes the large data source of the BrainMap database and identifies significant areas of above-chance co-activation with the seed-region via the activation-likelihood-estimation approach. In order to delineate functional networks formed by cortical as well as striatal atrophy regions we computed the conjunction between the co-activation profiles of striatal and cortical seeds in the premanifest and manifest stages of HD, respectively. Functional characterization of the seeds was obtained using the behavioral meta-data of BrainMap. Cortico-striatal atrophy seeds of the premanifest stage of HD showed common co-activation with a rather cognitive network including the striatum, anterior insula, lateral prefrontal, premotor, supplementary motor and parietal regions. A similar but more pronounced co-activation pattern, additionally including the medial prefrontal cortex and thalamic nuclei was found with striatal and IFJ seeds at the manifest HD stage. The striatum and M1 were functionally connected mainly to premotor and sensorimotor areas, posterior insula, putamen and thalamus. Behavioral characterization of the seeds confirmed that experiments activating the MOG or IFJ in conjunction with the striatum were associated with cognitive functions, while the network formed by M1 and the striatum was driven by motor-related tasks. Thus, based on morphological changes in HD, we identified functionally distinct cortico-striatal networks resembling a cognitive and motor loop, which may be prone to early disruptions in different stages of the disease and underlie HD-related cognitive and motor symptom profiles. Our findings provide an important link between morphometrically defined seed-regions and corresponding functional circuits highlighting the functional and ensuing clinical relevance of structural damage in HD.

1. Introduction

Huntington's disease (HD) is an autosomal-dominantly inherited neurodegenerative disorder caused by an expansion of CAG repeats on chromosome 4p and clinically characterized by a complex phenotype encompassing a triad of motor, psychiatric and cognitive dysfunctions. The neuropathological hallmark of HD is progressive degeneration of the striatum detectable up to two decades prior to the onset of the

first motor symptoms and leading to widespread brain atrophy with disease progression (Aylward et al., 2004; Paulsen et al., 2010; Tabrizi et al., 2011, 2012, 2013).

Structural brain imaging measures, particularly the assessment of caudate atrophy, have been shown to be predictive of symptom onset and in tracking disease progression (Aylward et al., 2011; Tabrizi et al., 2009, 2011, 2012, 2013). However, the search for reliable and clinically meaningful biomarkers in HD is accompanied by a better understanding of the relationship between (regional) brain volume loss and its contribution to the emergence of clinical symptoms. Importantly, disease-related behavioral manifestations are less likely to be sufficiently explained by distinct regional tissue degeneration, but rather depend on the complex interactions within multiple brain circuits or disruptions of the same — emanating from or even beginning before overt structural atrophy. Hence, the multimodal analysis of dynamic networks and connectivity dysfunctions along with neural cell loss may offer a more comprehensive understanding of the complex neuropathology underlying the heterogeneous nature of HD (Georgiou-Karistianis, 2009; Paulsen, 2009). Particularly in the premanifest stage of HD, where cognitive and psychiatric disturbances seem to precede the motor diagnosis (Paulsen et al., 2006; Paulsen, 2011), characterization of aberrant functional networks has been shown to be more sensitive to detect the earliest changes in HD than those in structural imaging alone (Wolf et al., 2007; Wolf et al., 2008b). Moreover, in manifest HD, when striatal volume loss has already progressed and the degenerative process afflicts widespread brain regions, and thus cortico-striatal projections, the clinical picture becomes more heterogeneous. This raises the need for an appropriate functional differentiation between multiple behavioral outcomes on the neural level and for a better characterization of alterations within these networks in different stages of the disease.

In recent years a number of task-based and resting-state imaging studies have investigated functional connectivity changes in HD, if at all mostly after controlling for or partialling out gray matter atrophy (e.g., Dumas et al., 2013; Werner et al., 2014), and only a few addressing the impact of regional volume loss on functional connectivity (Quarantelli et al., 2013; Wolf et al., 2014). However, as functional network connectivity inherently depends on tissue integrity, network analysis based on local volume destruction may predict deviation from normal brain performance due to structural degeneration and enable insights into the underlying neuronal dysfunctions. Modeling of networks co-activating with (or functionally connected to) HD-specific consistently atrophied areas may therefore contribute to a more comprehensive understanding of structural alterations and the complex clinical picture presented in HD. In addition, functional network analysis related to structural damage in HD may increase the predictive value of structural imaging methods by enhancing our knowledge on the ensuing clinical relevance of HD-related tissue destruction. This would ultimately offer a framework to monitor disease progression within these networks and associated clinical manifestations.

In order to synthesize structural magnetic resonance imaging (MRI) findings across the whole brain, we recently performed a coordinate-based meta-analysis of voxel-based morphometry (VBM) studies in HD and delineated a consistent pattern of brain atrophy across studies in premanifest and early manifest patients (Dogan et al., 2013). While marked striatal atrophy was shown to be evident in premanifest HD, we also observed involvement of cortical degeneration in the premanifest stage, particularly in the occipital cortex. After symptom manifestation, which is conventionally defined by the onset of motor symptoms, cerebral atrophy was more pronounced and cortically more widespread. While higher numbers of CAG repeats were associated with striatal degeneration, parameters of disease progression and motor impairment additionally correlated with cortical atrophy, especially in sensorimotor areas (Dogan et al., 2013). We argued that this pattern of structural degeneration may underlie the heterogeneous phenotype in HD and emphasized the need to extend the focus of research from the key region of neuropathology (i.e., degeneration of

the striatum) to a more differentiated picture of cortical–subcortical changes and potential disturbances in the networks formed by these regions.

Therefore, our aim in the current study was to functionally characterize the consistent pattern of brain atrophy as observed in our meta-analysis and to probe the ensuing clinical relevance of structural damage in HD. For this, we considered atrophied areas as nodes within dynamic networks and performed functional connectivity analyses to detect which brain areas co-activate with these regions. Connectivity analyses included both a task-based approach via the new neuroimaging tool "meta-analytic connectivity modeling" (MACM) as well as a task-free resting-state functional MRI (fMRI). By combining both task-driven and task-independent connectivity modeling tools we aimed to investigate convergent functional networks in different states of brain functioning as well as at rest. In order to integrate connectivity findings and ensuing behavioral correlates, we additionally assessed behavioral domains and paradigm classes associated with regions of consistent atrophy. Connectivity modeling and behavioral decoding of atrophied areas were applied in the following way: As a hallmark of the disease, we were first interested in i) co-activation profiles related to striatal volume loss known to be affected early on in HD. Convergent clusters of striatal atrophy were retrieved from our meta-analysis and used as seeds for functional connectivity modeling. Since the striatum is a key structure in the brain involved in a broad variety of functions, we expected to find a widespread functional network co-activating with HD-related striatal atrophy areas. In a further step we wanted to delineate functional networks formed by both striatal as well as cortical atrophy regions in different stages of the disease, as these networks would be in particular prone to early disease-related disruptions. That is, we considered those brain regions showing common co-activation with both the striatal and cortical atrophy areas. Given that these regions would be connected to atrophy nodes cortically as well as subcortically and therefore highly vulnerable to network disturbances, we aimed to achieve a more reliable inference on the functional role of HD-specific brain structure changes (instead of assessing co-activation profiles separately for each atrophy seed). Thus, we performed functional connectivity modeling of cortical in conjunction with striatal atrophy seeds retrieved from the meta-analysis at the ii) premanifest and iii) manifest HD stages. We hypothesized that connectivity analysis of the cortico-striatal seeds in the premanifest HD stage would reveal a network which mirrors the cognitive disturbances presented at this disease stage, while the seeds of the manifest stage would show more widespread network involvement reflecting cognitive and motor dysfunctions in clinical HD.

2. Methods

2.1. Seed regions: meta-analysis of consistent neurodegeneration in HD

In a recent coordinate-based meta-analysis of VBM studies in HD (Dogan et al., 2013) we identified the core regions of consistent neurodegeneration in premanifest and manifest HD mutation carriers. Drawing on these results, our aim in the current study was to functionally characterize this pattern of brain atrophy and to identify functional networks co-activating with these atrophic regions (seeds) and most likely being disrupted early in HD. Since degeneration of the striatum is the early pathognomonic key marker of the neurodegenerative process in HD, first we performed functional connectivity analysis of convergent striatal atrophy as observed in our meta-analysis encompassing 685 HD mutation carriers and 507 healthy controls. That is, we computed the conjunction between co-activation profiles of the left and right striatal atrophy seeds (cluster volumes: right 5872 mm^3; left 6880 mm^3; Fig. 1A).

Second, we were interested in modeling networks co-activating with both striatal and cortical atrophy regions in different HD stages, hence being in particular vulnerable to disease-related disruptions.
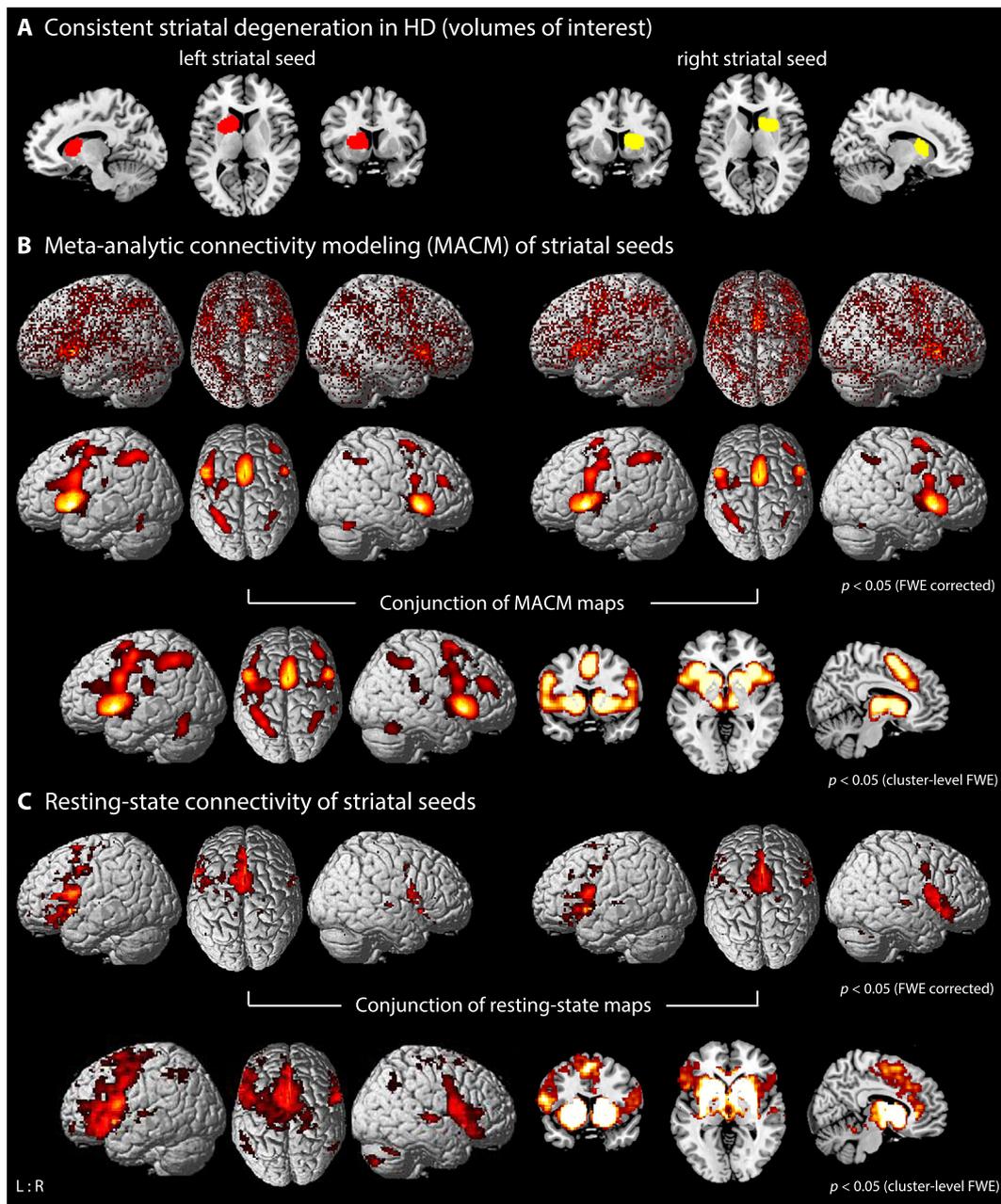
Fig. 1. Functional connectivity modeling of consistent striatal atrophy in HD. A) Location of the left (cluster maxima [x/y/z in MNI]: −12/12/6) and right (24/8/8) striatal seeds showing convergent evidence of atrophy as revealed by coordinate-based meta-analysis across voxel-based morphometry studies in HD (Dogan et al., 2013). B) Brain-wide co-activation maps of the seed regions as revealed by MACM: 1st panel: Brain-wide foci reported in BrainMap that featured the activation peaks closest to the respective seed voxels; these foci are modeled by 3D Gaussian reflecting uncertainty of their location using ALE meta-analysis. 2nd panel: above-chance convergence indicates significant co-activations with the respective seed region. 3rd panel: conjunction analysis showing common brain-wide co-activations between the left and right striatal seeds. C) 1st panel: resting-state connectivity for the left and right striatal seeds, respectively. 2nd panel: conjunction analysis showing common resting-state connectivity between the left and right striatal seeds.

Meta-analysis of VBM studies in premanifest HD yielded convergent volume reductions in the striatum (*right* 13,208 mm^3; *left* 11,768 mm^3; Fig. 2A.1), as well as in the right middle occipital gyrus (MOG; 2048 mm^3; Fig. 2A.1). These atrophy seeds in the premanifest stage of HD (left or right striatum in conjunction with MOG) were combined and used for functional connectivity modeling as described below.

Finally, in the early manifest stage of HD, cerebral atrophy was more pronounced and spread to cortical regions, bilaterally in the striatum (*right* 6344 mm^3; *left* 5144 mm^3; Fig. 2A.2), motor cortex (M1; *right* 1496 mm^3; *left* 3128 mm^3; Fig. 2A.2) and inferior frontal junction (IFJ;

right 1904 mm^3; *left* 1848 mm^3; Fig. 2A.2). Both striatal and cortical seeds, separately for IFJ and M1, were again combined and the common functional connectivity profiles related to these seeds were computed via conjunction analyses (please see Supplementary Fig. S1 for a detailed overview of our workflow).

2.2. Meta-analytic connectivity modeling (MACM)

Task-based functional connectivity of convergent atrophy seeds (Fig. 1A, Fig. 2A) was assessed using meta-analytic connectivity modeling (MACM) based on the BrainMap database (http://www.brainmap.
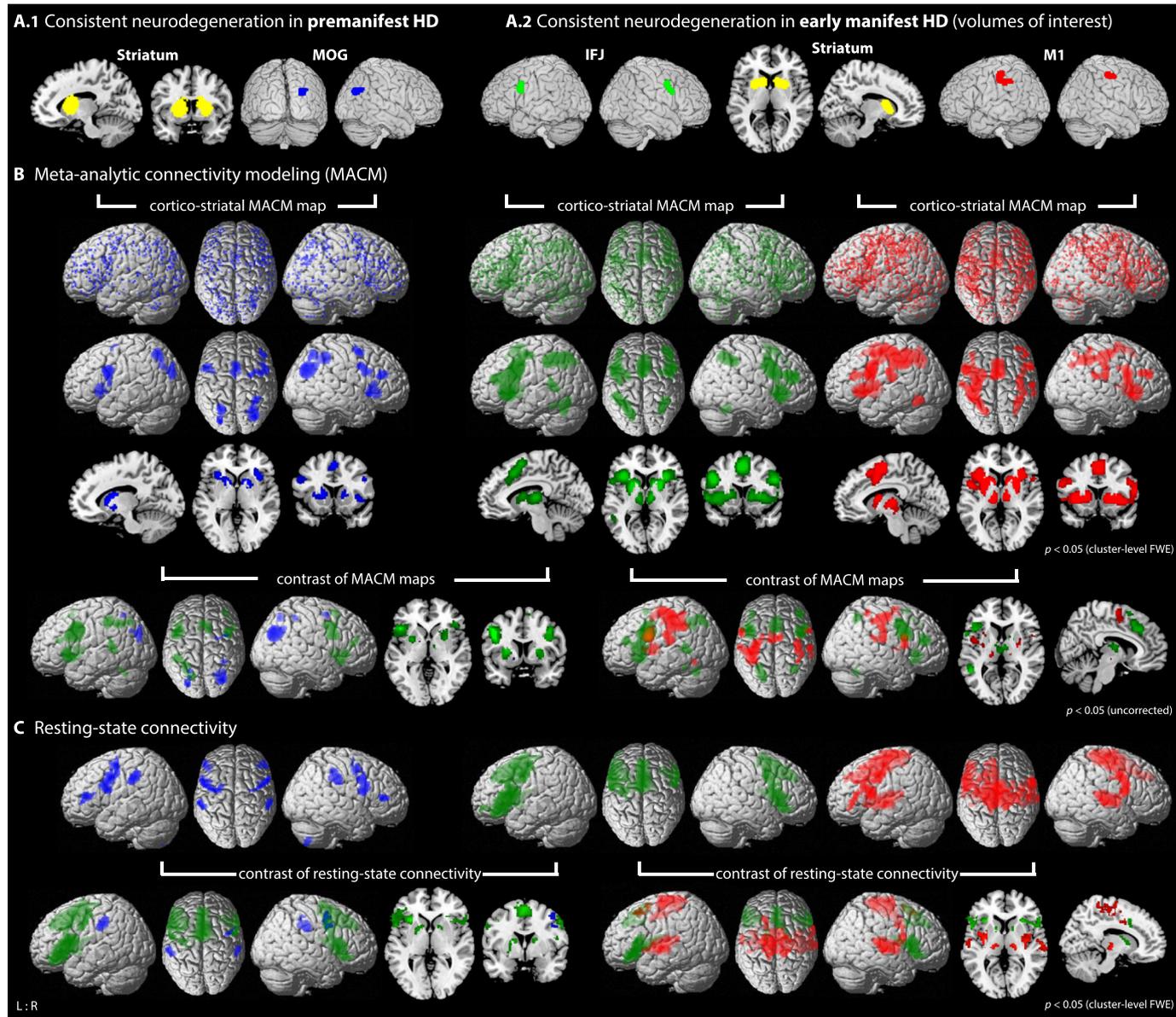
Fig. 2. Functional connectivity modeling of consistent cortico-striatal atrophy in premanifest and manifest HD. A) Location of the seed regions showing convergent evidence of atrophy as revealed by coordinate-based meta-analysis across voxel-based morphometry studies in HD (Dogan et al., 2013): A.1 in premanifest HD located in the striatum (cluster maxima [x/y/z in MNI]: *right* 26/8/8; *left* −32/−12/−8 and −14/6/14) and right middle occipital gyrus (MOG; 30/−72/28); A.2 in manifest HD located in the striatum (*right* 24/6/10; *left* −10/12/8), inferior frontal junction (IFJ; right 40/2/38; left −42/8/28) and motor cortex (M1; *right* 34/−24/52; *left* −34/−28/52). B) Brain-wide co-activation maps of the respective cortical seeds in conjunction with striatal seeds as revealed by MACM (*blue*: MOG-striatal map; *green*: IFJ-striatal map; *red*: M1-striatal map): 1st panel: Brain-wide foci reported in BrainMap that featured the activation peaks closest to the respective seed voxels; these foci are modeled by 3D Gaussian reflecting uncertainty of their location using ALE meta-analysis. 2nd/3rd panel: above-chance convergence indicates significant co-activations with the respective seed region. 4th panel: contrast analysis between MACM maps showing differences in brain-wide co-activations patterns (*blue*: MOG-striatal map > IFJ-striatal map; *green — left side*: IFJ-striatal map > MOG-striatal map; *green — right side*: IFJ-striatal map > M1-striatal map; *red*: M1-striatal map > IFJ-striatal map). C) 1st panel: resting-state connectivity of the respective cortical seeds in conjunction with striatal seeds. 2nd panel: contrast analysis between resting-state connectivity (see above for color coding).

org; Laird et al., 2009a, 2011). MACM assesses the brain-wide co-activation pattern of an anatomical region across a large number of functional neuroimaging results and identifies significant areas showing above-chance co-activation with this seed region. This convergence is obtained by applying the 'activation likelihood estimation' approach (ALE) over the co-activation foci derived from BrainMap (Eickhoff et al., 2012; Fox et al., 2014). The rationale behind MACM to assess inter-regional connectivity is conceptually similar to functional non-meta-analytic approaches (e.g., resting state fMRI) by using temporal co-variations in regional activation to detect connectivity. Whereas in a typical fMRI study the unit of time is the second, in the meta-analytic approach the unit of time is the study or experiment. Regions in which activations co-occur consistently across studies (i.e., regions that are mutually predictive) indicate functionally connected areas with higher probability of co-occurrence reflecting greater strength of functional connectivity. Hence, MACM bases on the probability of co-occurrence of neuronal activation between regions over a broad range of tasks and mental operations, revealing those networks that are con-jointly and consistently recruited across studies. These co-activations can be regarded as the meta-analytic correlate of functional connectiv-ity (Wager et al., 2009).

The first step in MACM is to identify all experiments in BrainMap reporting at least one focus of activation in healthy subjects in the seed region (Fig. 1B). Currently, coordinate-based results (in Talairach or MNI space) of over 11,000 functional neuroimaging experiments are stored in the BrainMap database. To avoid a pre-selection bias and enable a completely data-driven approach, all eligible BrainMap exper-iments independent of behavioral categories were considered. The subsequent quantitative ALE meta-analysis tests for convergence across the foci derived from BrainMap indicating consistent co-activation (i.e., task-based functional connectivity) with the respective seed (Eickhoff et al., 2009, 2010, 2012; Laird et al., 2009a; 2009b; Turkeltaub et al., 2002, 2012).

The ALE algorithm aims at identifying areas showing a convergence of reported coordinates across experiments, which is higher than ex-pected under a random spatial association. The key idea is to treat the reported foci not as single points, but rather as centers of three-dimensional Gaussian probability distributions capturing the spatial un-certainty associated with each focus based on an empirical model of between-subject and between-template variance (Eickhoff et al., 2009). The probabilities of all foci reported in the given experiments were then combined for each voxel, resulting in a modeled activation (MA) map (Turkeltaub et al., 2012). Taking the union across these MA maps yielded voxel-wise ALE scores describing the convergence of re-sults at each particular location of the brain. To distinguish 'true' conver-gence between studies from random convergence (i.e., noise), ALE scores were compared to an empirical null-distribution (Eickhoff et al., 2012) reflecting a random spatial association between experiments. Hereby, a random-effects inference is invoked, focusing on inference on the above-chance convergence between experiments, not clustering of foci within a particular study. The p-value of a "true" ALE was then given by the proportion of equal or higher values obtained under the null-distribution (Eickhoff et al., 2012). The resulting non-parametric p-values for each meta-analysis were then thresholded at $p < 0.05$, with any significant convergence outside the seed region reflecting con-sistent convergence of co-activations, i.e., task-based functional connec-tivity, since experiments featuring at least one focus of activation in the respective seed were entered in the analysis.

In order to assess significant functional connectivity with areas of convergent HD-related striatal atrophy (Fig. 1A), we first performed MACM analysis with the left and right striatal seeds derived from the meta-analysis across all HD studies. For this, we computed the conjunc-tion between the left and right striatal connectivity maps using the min-imum statistics (Nichols et al., 2005) thresholded at a cluster-level family-wise error (FWE) corrected $p < 0.05$ (cluster-forming threshold at voxel-level $p < 0.001$). To detect disease-related brain networks

showing common connectivity with altered striatal and cortical struc-tures in HD, we first identified all eligible experiments in the BrainMap database that reported at least one focus of activation in the striatal in conjunction with the cortical atrophy seed (Fig. 2A). That is, for atrophy seeds derived from the meta-analysis across premanifest HD studies (see above), we performed MACM analysis across experiments activat-ing both (left or right) striatal and the right MOG seeds and used ALE meta-analysis to identify consistent co-activations as reported in the retrieved experiments. Thus, the resulting functional connectivity map (i.e., MOG-striatal map) would not only be formed by HD-related striatal but also cortical atrophy consistently observed in the premanifest stage of HD. In order to delineate cortico-striatal network alterations in early manifest HD, task-based co-activation was assessed across experiments activating striatal and IFJ seeds and, in a separate analysis, striatal and M1 seeds (i.e., [(left or right) striatal seed AND (left or right) cortical seed]). All analyses were thresholded at a cluster-level FWE corrected $p < 0.05$ ($p < 0.001$ at the voxel-level). Hereby, we aimed at identifying functionally distinct networks that might be associated with early de-generation of the striatum as well as of either prefrontal or motor func-tioning in HD (IFJ-striatal, M1-striatal maps; see also Supplementary Fig. S1).

Finally, to contrast the functional connectivity networks derived from the cortico-striatal seed areas (i.e., co-activation maps of both striatal and cortical atrophy in HD), we first calculated the voxel-wise differences of the Z-scores obtained from the respective MACM-maps (i.e., MOG-striatal, IFJ-striatal, M1-striatal maps). The experiments con-tributing to either analysis were then pooled and randomly divided into two groups of the same size as the sets of contrasted experiments (Eickhoff et al., 2011). Voxel-wise ALE scores for these two randomly assembled groups were subtracted from each other and recorded. Repeating this process 10,000 times yielded an empirical null distribu-tion of ALE-score differences between the two conditions. Based on this permutation-procedure, the map of true differences was then thresholded at a posterior probability of $p > .95$ for a true difference be-tween the two samples (cluster extend threshold $k_E \geq 100$ voxels; cf. Rottschy et al., 2013).

2.3. Task-independent "resting-state" connectivity

Resting-state fMRI images of 132 healthy volunteers (mean age 42.3 ± 18.1 SD years; 78 male) without records of neurological or psy-chiatric disorders were obtained from the NKI/Rockland sample (Nooner et al., 2012). During the resting-state scans the subjects were instructed to keep their eyes closed and to think about nothing in partic-ular but not to fall asleep (which was confirmed by post-scan debriefing). For each subject 260 resting-state EPI images were acquired on a Siemens Tim Trio 3 T scanner using blood-oxygen-level-dependent (BOLD) contrast [gradient-echo EPI pulse sequence, TR = 2.5 s, TE = 30 ms, flip angle = 80°, in plane resolution = 3.0×3.0 mm^2, 38 axial slices (3.0 mm thickness) covering the entire brain]. The first four scans were excluded from further processing analysis using SPM8 (http://www.fil.ion.ucl.ac.uk/spm/). The EPI images were first corrected for movement artifacts by affine registration using a two pass procedure in which the images were first aligned to the initial volumes and subse-quently to the mean after the first pass. The obtained mean EPI of each subject was then spatially normalized to the MNI single subject template using the 'unified segmentation' approach (Ashburner and Friston, 2005). The ensuing deformation was applied to the individual EPI volumes. To improve signal-to-noise ratio and compensate for resid-ual anatomical variations, images were smoothed by a 5-mm FWHM Gaussian.

The time-series data of each voxel were processed as follows (Eickhoff et al., 2011; Zu Eulenburg et al., 2012): In order to reduce spu-rious correlations, variance that could be explained by the following nuisance variables was removed: i) the six motion parameters derived from the image realignment, ii) the first derivative of the realignment

parameters, and iii) mean gray matter, white matter and CSF signal per time-point as obtained by averaging across voxels attributed to the respective tissue class in the SPM8 segmentation. All nuisance variables entered the model as first and second order. Data were then band pass filtered preserving frequencies between 0.01 and 0.08 Hz, since meaningful resting-state correlations will predominantly be found in these frequencies given that the bold-response acts as a low-pass filter (Biswal et al., 1995; Fox and Raichle, 2007).

We used the same seed regions as for the MACM analysis, i.e., the clusters of convergent atrophy obtained from the meta-analysis, and performed conjunction analyses of resting-state co-activations between striatal and cortical seeds (MOG-striatal, IFJ-striatal, M1-striatal maps). Linear (Pearson) correlation coefficients between the time series of the seed regions and all other gray matter voxels in the brain were computed to quantify resting-state functional connectivity (Reetz et al., 2012). These voxel-wise correlation coefficients were then transformed into Fisher's Z-scores and tested for consistency across subjects in a random-effects analysis after accounting for subjects' age as a nuisance regressor. In correspondence with the MACM co-activation analysis described above, we first assessed resting-state connectivity using HD-related (left and right) striatal atrophy as seeds (Fig. 1A). In order to delineate task-free functional connectivity shared by both striatal and cortical atrophy seeds (i.e., MOG-striatal, IFJ-striatal, M1-striatal maps), we then performed conjunction analyses (Nichols et al., 2005) between resting-state connectivity of striatal and cortical clusters, using premanifest and manifest atrophy regions respectively (Fig. 2A). Analogous to MACM, the results were thresholded at a cluster-level FWE corrected $p < 0.05$ (cluster-forming threshold at voxel-level $p < 0.001$). Finally, resting-state co-activation maps of the different cortico-striatal seeds were contrasted using exclusive masking (uncorrected mask at $p < 0.05$) and thresholded at a cluster-level FWE corrected $p < 0.05$ ($p < 0.001$ at the voxel-level).

2.4. Cross-validation of task-based and task-free functional connectivity

In order to identify consistent functional connectivity maps showing both task-based and task-independent co-activation with the seed regions, we performed conjunction analyses between MACM and resting-state analysis using the minimum statistics (Nichols et al., 2005). That is we computed the intersection between the connectivity maps of both analyses identifying those areas that showed significant functional connectivity with the cortico-striatal seed regions in task-dependent as well as task-independent states (Reetz et al., 2012; Rottschy et al., 2013). The results of these consensus maps between MACM and resting-state connectivity were thresholded at a cluster-level FWE corrected $p < 0.05$ ($p < 0.001$ at the voxel-level).

2.5. Anatomical allocation

Results were anatomically labeled by reference to probabilistic cytoarchitectonic maps of the human brain using the SPM Anatomy Toolbox (Eickhoff et al., 2005; Eickhoff et al., 2007). Using a Maximum Probability Map (MPM), activations were assigned to the most probable histological area at their respective locations. Details on these cytoarchitectonic regions can be found in the following publications reporting on the cerebellum (Diedrichsen et al., 2009), thalamic connectivity zones (Behrens et al., 2003), amygdala (Amunts et al., 2005), Broca's area (Brodmann areas [BA] 44, 45; Amunts et al., 1999), premotor cortex (PMC, BA 6; Geyer, 2004), primary motor cortex (M1, BA 4a, 4p; Geyer et al., 1996), primary somatosensory cortex (SI, BA 3, 1, 2; Geyer et al., 1999; Geyer et al., 2000), secondary somatosensory cortex (SII: OP1, OP4; Eickhoff et al., 2006), inferior and superior parietal cortices (IPC, SPL; Caspers et al., 2008; Scheperjans et al.,

2008), intraparietal sulcus (IPS; Choi et al., 2006; Scheperjans et al., 2008), and posterior insula (Kurth et al., 2010a).

2.6. Behavioral characterization

In order to functionally characterize our morphometrically defined seed regions and to potentially differentiate corresponding brain networks on a behavioral level, we used the metadata of BrainMap describing each neuroimaging experiment included in the database. Behavioral domains code the specific mental process isolated by the statistical contrast of each archived neuroimaging experiment (Laird et al., 2011) and include the main categories of cognition, action, perception, emotion, interoception, as well as their related subcategories. The respective paradigm classes classify the specific task employed (a complete list of BrainMap's taxonomy comprising behavioral domains and paradigm classes can be found at http://brainmap.org/scribe/). We analyzed the behavioral domain and paradigm class metadata associated with each of our premanifest and manifest atrophy seed regions by computing conditional probabilities of observing activation in a region given a particular behavioral domain or paradigm class, and *vice versa* (forward and reverse inference). As individual regions participate in multiple cognitive operations and a single elementary process involves multiple regions, we used both functional decoding approaches aiming to relate defined psychological processes to the examined brain areas instead of ascribing a unique role of a brain region in a certain mental process. Forward inference is the probability of observing activity in a brain region given knowledge of the psychological process [P(*Activation | domain or paradigm*)], whereas reverse inference is the probability of a psychological process being present given knowledge of activation in a particular brain region [P(*domain or paradigm | Activation*)] (cf. Clos et al., 2013; Rottschy et al., 2013). The functional roles of the seeds were identified by significant over-representation of behavioral domains and paradigm classes in the experiments activating the respective seed region relative to the overall chance of finding activation in that particular seed across the BrainMap database using a binomial test at $p < 0.05$, Bonferroni corrected for multiple comparisons (Eickhoff et al., 2011; Laird et al., 2009a). For the reverse inference, a seed's functional profile was determined by identifying the most likely behavioral domains and paradigm classes given activation in a particular cluster. This likelihood P(*domain or paradigm | Activation*) can be derived from P(*Activation | domain or paradigm*) as well as P(*domain or paradigm*) and P(*Activation*) using Bayes rule. Significance was then assessed by means of a chi-squared test ($p < 0.05$, Bonferroni corrected for multiple comparisons).

In order to characterize the functional profile of our selective cortico-striatal networks using premanifest and manifest atrophy seeds, we filtered BrainMap data for those experiments activating both the (left or right) striatal in conjunction with the respective (left or right) cortical seeds, thresholded at $p < 0.01$ (uncorrected).

3. Results

3.1. Functional connectivity modeling of consistent striatal atrophy in HD

MACM of both left and right striatal seeds (Fig. 1A) showed significant task-based connectivity mainly within the basal ganglia (caudate nucleus, putamen, globus pallidus), the thalamus, amygdala, insula, inferior frontal gyrus (including Broca's area), premotor cortex (PMC), supplementary motor area (SMA) and primary motor cortex (M1), mid-cingulate cortex (MCC), inferior parietal cortex (IPC), intraparietal sulcus (IPS) and posterior cerebellum (Fig. 1B; please see Supplementary Table S1 for a detailed description of significant clusters and anatomical areas).

A similar co-activation pattern was observed in the resting-state connectivity analysis, showing additional connectivity with the anterior cingulate cortex and to a lesser extent parietal connectivity (Fig. 1C; Table S1). Conjunction analysis between MACM and resting-state connectivity showed a common map comprising bilaterally the basal

ganglia, thalamus, amygdala, insula, inferior frontal gyrus, M1, PMC, SMA and MCC (Table S1).

3.2. Functional connectivity and behavioral characterization of consistent cortico-striatal atrophy in premanifest HD

MACM analysis of consistent neurodegeneration in premanifest HD was performed with striatal seed regions in conjunction with the right MOG (Fig. 2A.1), which revealed significant co-activations with a network comprising bilaterally the caudate nucleus, ventral putamen, globus pallidus, anterior insula, inferior frontal gyrus (overlapping with BA 44), right middle and superior frontal gyri, bilateral SMA, IPS, superior parietal lobule (SPL) and MOG (Fig. 2B; Table S2).

Resting-state connectivity analysis of consistent MOG-striatal atrophy in premanifest HD resulted in a map consisting of Broca's area (BA 44, 45), superior frontal gyrus, PMC, IPC and right posterior cerebellum (Fig. 2C; Table S2). Conjunction of both MACM and resting-state connectivity revealed the dorsolateral prefrontal cortex (DLPFC) as a common area of co-activation (Fig. 3A; Table S2).

Behavioral characterization of premanifest atrophy seeds based on the BrainMap database showed that the striatal regions were associated with a broad range of behavioral domains, including cognition, emotion, action–execution and pain perception, and paradigm classes such as reward tasks, movement-related task, pain monitoring and discrimination (Supplementary Fig. S2A). The right MOG seed was rather related to the cognitive and visual perception domains and involved in working memory, and executive and mental rotation paradigms (Fig. S2A). Since our main interest in the current analysis was focused on functional associations related to both striatal and cortical atrophy, we filtered the BrainMap data for those experiments activating both the (left and right) striatal in conjunction with the right MOG seeds. Here, we found significant associations with cognitive domains (reasoning, working memory) as well as reward paradigm classes, while the reverse

inference for the probability of certain paradigm classes given activation in these seeds was not significant (Fig. 4A).

3.3. Functional connectivity and behavioral characterization of consistent cortico-striatal atrophy in early manifest HD

3.3.1. MACM of manifest atrophy seeds

MACM of the IFJ in conjunction with the striatal seeds (Fig. 2A.2) revealed a map including bilaterally the basal ganglia, thalamus (mainly the prefrontal and temporal connectivity zones; Behrens et al., 2003), anterior insula, inferior frontal gyrus (including Broca's area), SMA, MCC, superior medial gyrus, IPS, SPL, posterior cerebellum and fusiform gyrus, left IPC and middle temporal gyrus. MACM of M1-striatal seeds showed significant co-activation bilaterally with the basal ganglia, thalamus, insula, inferior frontal gyrus (BA 44), MCC, SMA, PMC, M1, primary somatosensory cortex (SI), parietal cortex (IPS, IPC, SPL) as well as parietal operculum (Fig. 2B; Table S3). Contrasting both MACM maps the IFJ-striatal map, compared to the M1-striatal map, showed more co-activation with the dorsal caudate nucleus, thalamic nuclei connecting to the temporal and prefrontal cortices, anterior insula, Broca's area, middle frontal gyrus, superior medial frontal gyrus, MCC, SMA, SPL, IPS, left middle temporal gyrus and posterior cerebellum. In contrast, the M1-striatal seeds co-activated the putamen, pallidum, left thalamus connecting mainly to the (pre-)motor and parietal regions, left posterior insula, bilateral inferior frontal gyrus (BA 44), SMA, PMC, M1, SI, IPC, parietal operculum (SII) and left IPS (Fig. 2B; Table S3).

3.3.2. Resting-state connectivity of manifest atrophy seeds

Similarly to MACM, resting-state connectivity analysis of the IFJ-striatal seeds showed co-activation with the dorsal caudate nucleus, left putamen and thalamus connecting to the prefrontal cortex, bilateral anterior insula, inferior frontal gyrus including Broca's area, superior medial gyrus, SMA and PMC. These regions (except for the PMC) also
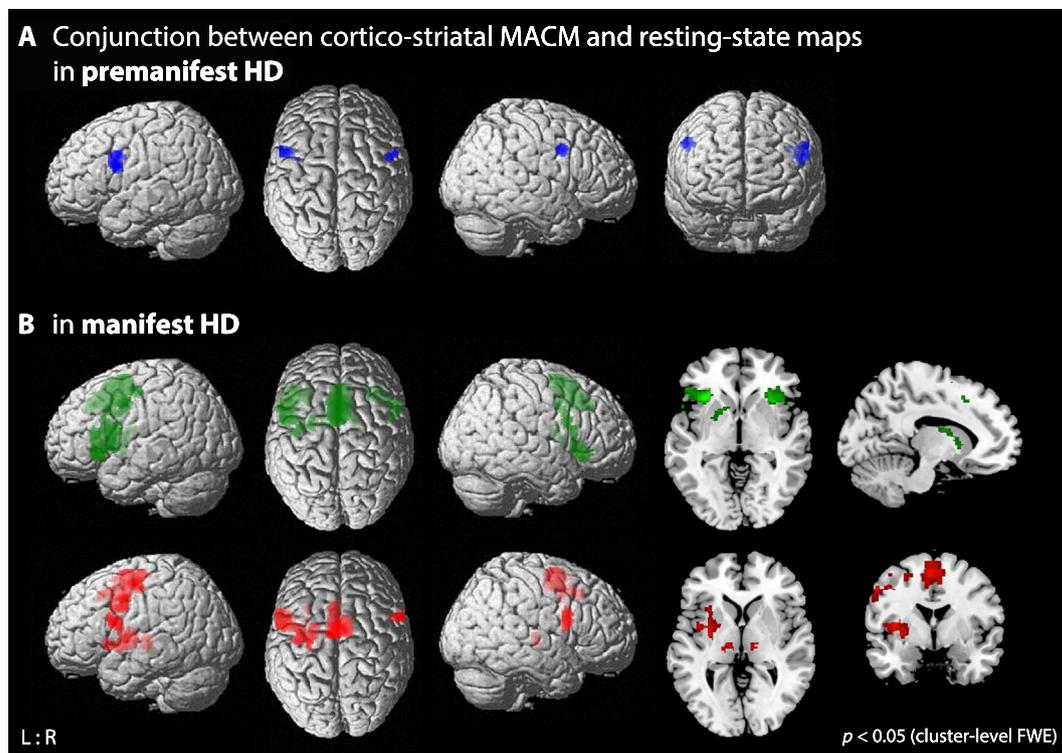

Fig. 3. Conjunction analysis between MACM and resting-state connectivity maps of consistent cortico-striatal atrophy in premanifest and manifest HD. A) Conjunction across MACM and resting-state connectivity maps of consistent MOG-striatal atrophy in premanifest HD (*blue*). B) Conjunction across MACM and resting-state connectivity maps of consistent IFJ-striatal (*green*) and M1-striatal (*red*) atrophy in manifest HD.

A Functional characterization of **premanifest seeds** (striatum & MOG)
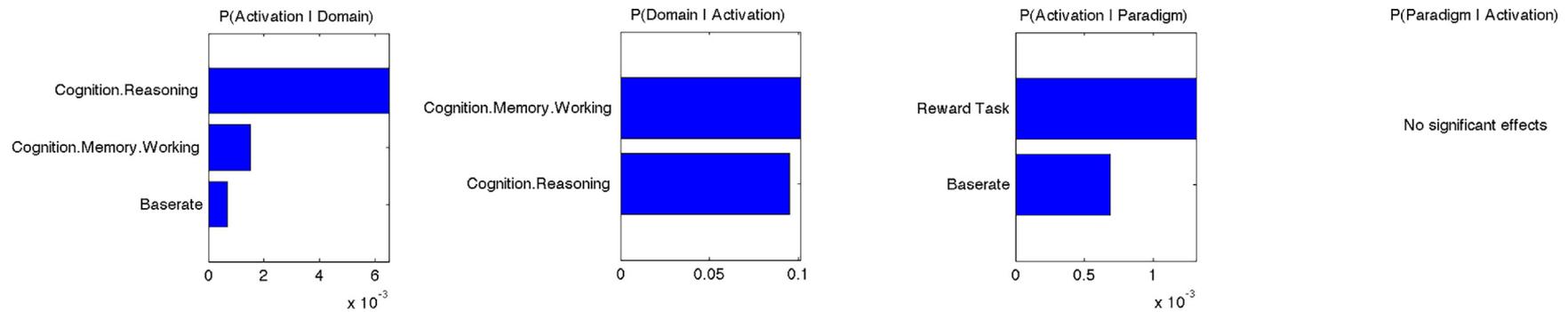
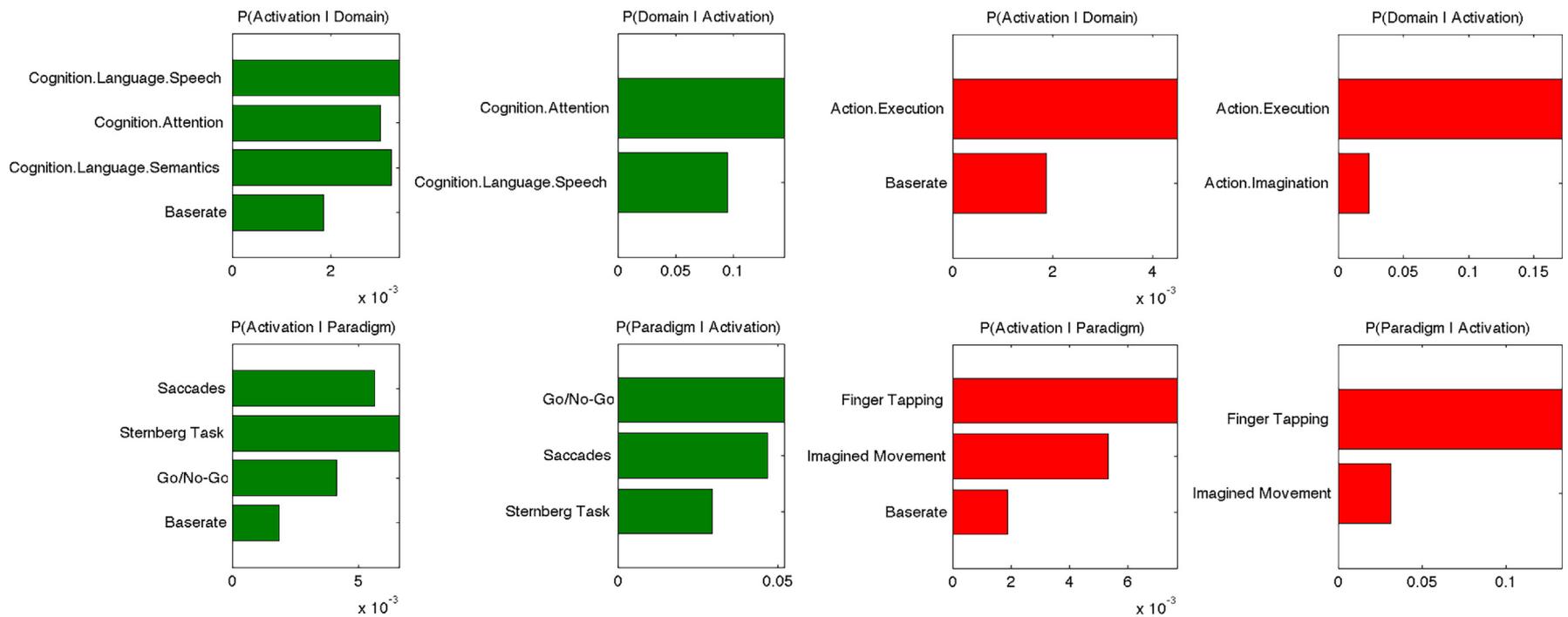**B** Functional characterization of **manifest seeds** (striatum & IFJ / M1)

Fig. 4. Functional characterization by behavioral domains and paradigm classes. A) Functional characterization by behavioral domains and paradigm classes of MOG-striatal atrophy seeds in premanifest HD (*blue*). B) Functional characterization by behavioral domains and paradigm classes of IFJ-striatal (*green*) and M1-striatal (*red*) atrophy seeds in manifest HD. Bar plots show significant associations (at $p < 0.01$, uncorrected) of behavioral domains and paradigm classes from the BrainMap meta-data given observed brain activity (and *vice versa*); the *x*-axis indicates relative probability values.

showed stronger connectivity with the IFJ-striatal map compared to the M1-striatal map. For the latter we observed co-activation across the brain with the bilateral putamen, mainly motor, premotor and somato-sensory thalamic nuclei, posterior insula, inferior frontal gyrus (BA 44), MCC, SMA, PMC, M1, parietal operculum (SII), Heschl's gyrus, superior temporal gyrus, left IPC, middle frontal gyrus and right SI. Except for the connectivity with Broca's area, this co-activation pattern was largely confirmed in the contrast analysis with the IFJ-striatal map (Fig. 2C; Table S4).

3.3.3. Conjunction between MACM and resting-state connectivity of manifest atrophy seeds

For the IFJ-striatal seeds, conjunction analysis between MACM and resting-state connectivity revealed a co-activation map comprising the bilateral caudate nucleus dorsally, left ventral putamen, bilateral anterior insula, Broca's area (BA 44), SMA extending to MCC, left PMC and middle frontal gyrus. For the M1-striatal seeds both MACM and resting-state analyses showed common connectivity with the bilateral thalamus, SMA, BA 44, left PMC, M1, putamen and insula (Fig. 3B; Table S5).

3.3.4. Behavioral characterization of manifest atrophy seeds

Behavioral characterization of manifest atrophy seeds showed that striatal seeds (similar to the results reported for premanifest atrophy seeds) were related to the behavioral domains of cognition, emotion, action–execution and pain perception (Fig. S2B). While the profile of the left IFJ seed indicated a primary role in language-related processes such as phonology, semantics and speech, the right IFJ seed was rather related to attention and visual perception, and both left and right IFJ were involved in working-memory functions (Fig. S2B). The functional profile of both striatal in combination with IFJ atrophy seeds indicated significant associations with attention and language-related cognitive domains, and higher probabilities of activation elicited by paradigm classes such as Sternberg task, Go/No-Go and also saccades (Fig. 4B).

M1 atrophy seeds were mainly associated with action–execution and movement-related behavioral domains and paradigm classes (e.g., finger tapping), though the left M1 seed was also involved in tactile and sequence learning paradigm classes (Fig. S1B). M1 in conjunction with striatal seeds was driven by motor functions (execution and imagination of action) and experiments using finger tapping or imagined movements (Fig. 4B).

3.4. Comparison between premanifest and manifest maps

Due to similarities between the MOG-striatal and IFJ-striatal connectivity maps we additionally performed contrast analysis between these two maps (Fig. 2C; Table S6). Compared to manifest IFJ-striatal seeds, the MOG-striatal map showed task-based connectivity (MACM) only within the MOG, and resting-state connectivity in the IPC and right middle frontal gyrus. However, in the reversed contrast (MOG-striatal < IFJ-striatal) we found more extensive connectivity in the IFJ-striatal MACM map including the bilateral putamen, anterior insula, Broca's area, superior medial gyrus, SMA, MCC, right thalamus (prefrontal and temporal connectivity zones), caudate nucleus, left parietal regions (IPC, IPS, SPL), and middle and superior temporal gyri. Resting-state connectivity of IFJ-striatal seeds was similarly more widespread except for the parietal and temporal regions but additionally including the bilateral caudate nucleus, pallidum, PMC and left middle frontal gyrus (Fig. 2C; Table S6). We additionally compared the premanifest MOG-striatal with the manifest M1-striatal map (Table S7). Similarly, compared to the manifest M1-striatal seeds, the MOG-striatal map showed task-based connectivity within the MOG and SPL, and resting-state connectivity in the IPC and right middle frontal gyrus. The reversed contrast (MOG-striatal < M1-striatal), for both MACM and resting-state analyses, basically depicted the M1-striatal motor network as described above, including the putamen, posterior insula, premotor, sensorimotor and parietal regions (Table S7).

4. Discussion

Based on convergent morphological changes in HD, task-based MACM and task-free resting-state connectivity analyses identified functionally distinct, disease-stage dependent cortico-striatal networks, which may underlie the heterogeneous clinical picture in HD. Connectivity modeling of striatal seeds first revealed a widespread network including the basal ganglia, thalamus, amygdala, insula, prefrontal, and premotor and motor cortices emphasizing the involvement of the striatum in a broad variety of functions. In contrast, task-based and resting-state connectivity modeling of both striatal and cortical atrophy regions in premanifest HD was related to a rather circumscribed fronto-insular and parietal network associated with cognition that was also observed but more widespread in the manifest stage. Whereas the cognitive loop connects the caudate with frontal and parietal cortices, the connectivity pattern of the M1 seeds in conjunction with the striatum, as revealed for manifest HD exhibiting motor signs, resembles mainly the motor loop connecting the putamen with motor cortices and was also driven by motor tasks. These functionally segregated cognitive and motor networks based on convergent cortico-striatal atrophy in HD, and therefore prone to early disease-related disruptions, may account for the cognitive and motor symptom profiles at different stages of HD.

4.1. Functional connectivity of atrophy seeds in the premanifest HD stage

Functional connectivity modeling of early observed striatal in conjunction with occipital atrophy in premanifest HD mutation carriers, exhibiting no overt motor signs, was associated with cognitive functions such as working memory, reasoning and reward tasks, and revealed a network mainly consisting of the caudate nucleus, ventral putamen, anterior insula, lateral PFC, PMC, SMA and parietal regions. Working memory dysfunctions are one of the earliest cognitive domains known to be impaired in the premanifest stage of HD (Papp et al., 2011; Stout et al., 2011), and fronto-striatal circuits are particularly vulnerable in premanifest HD, which are closely related to the cognitive and psychiatric symptoms often preceding the onset of motor disorder in HD (Wolf and Kloppel, 2013). Interestingly, similar aberrant connectivity during a working-memory task was reported in premanifest HD mutation carriers including the left lateral PFC, parietal regions and bilateral striatum (Wolf et al., 2008b), as well as altered frontostriatal coupling with increasing cognitive demand (Wolf et al., 2008a). The DLPFC in particular seems to be a key region with respect to cognitive functioning in HD (Wolf et al., 2008a; Wolf et al., 2009), which could also be confirmed in our conjunction analysis between both MACM and resting-state maps showing the DLPFC as a common region functionally connected to cortico-striatal atrophy in the premanifest stage of HD. Moreover, the significance of altered DLPFC coupling during working memory performance in HD is also supported by the Australian IMAGE-HD study, a longitudinal neuroimaging study in both pre- and manifest HD, reporting increases in brain activity in premanifest mutation carriers, but reductions in functional connectivity between the DLPFC, caudate and parietal cortex over a period of 18 and 30 months (Georgiou-Karistianis et al., 2013; Poudel et al., 2015). These areas were also formed within the connectivity analysis of premanifest cortico-striatal atrophy functionally driven by working-memory tasks.

Cortico-striatal atrophy in premanifest HD was also functionally related to reward tasks suggesting an impact on mood symptomatology in HD. However, there is only sparse data on the functional correlates of psychiatric disturbances in HD. fMRI studies have mostly investigated the processing of emotional faces in both premanifest (Hennenlotter et al., 2004; Novak et al., 2012) and manifest HD (Dogan et al., 2014) showing widespread dysfunctions in neural, such as striatal, insular, prefrontal and parietal activity, consistent with the cortico-striatal premanifest map derived in our analysis. In particular, anterior insular and striatal alterations, both structurally and functionally, have been linked to impaired processing of negative emotions in HD (Henley et al., 2008;

Hennenlotter et al., 2004), which are one the earliest neuropsychologically detectable deficits in the premanifest stage (Paulsen, 2011).

Finally, only few studies have investigated task-free resting-state fMRI connectivity in premanifest HD basically being in accord with our resting-state connectivity map derived from early cortico-striatal atrophy. Dumas et al. (2013) reported reduced connectivity of left precentral, middle frontal, right parietal and cingulate gyri with a medial visual network in premanifest HD compared to controls, while in manifest HD connectivity of widespread brain regions with the default mode network (DMN) and executive control network was reduced (Dumas et al., 2013). In another analysis of the IMAGE-HD study using independent component analysis (ICA) of resting-state fMRI data, Poudel et al. (2014) found decreased synchrony within a sensorimotor network and in the lateral visual area of a dorsal attention network. Though the sensorimotor cortex was spared in our connectivity analysis in premanifest HD, involvement of the PMC (and SMA within MACM analysis) also indicated premature disruptions in motor circuits becoming more apparent in the manifest stage of HD. In accordance with this, Unschuld et al. (2012) assessed seed-based resting-state connectivity in premanifest-HD between the caudate and cortical seeds and found reduced cortico-striatal synchrony between the caudate and PMC related to striatal atrophy. Additionally, our data also showed significant resting-state connectivity of atrophy seeds in premanifest HD with the posterior cerebellum (lobule VIIb) known to be involved in cognitive functioning (Schmahmann, 1991). This suggests that early structural alterations in premanifest HD might also affect associative cortico-pontine inputs, which are conveyed in the posterior cerebellar lobe.

Overall, our task-based and resting-state connectivity map based on cortico-striatal atrophy in premanifest HD, which was functionally driven by cognitive tasks, widely depicts early alterations in functional connectivity in premanifest HD. It is important to note that our connectivity mapping approach was solely based on consistent brain structure changes in HD treating these areas as nodes within functional circuits that are particularly vulnerable to disease-related disruptions. Whereas striatal atrophy seeds showed relations to widespread brain areas (which is reasonable considering the striatum's role in cortico-striatal circuits), the circumscribed coactivation profile related to both striatal and occipital atrophy seeds revealed a comprehensive network for the premanifest stage of HD, in which cognitive and psychiatric impairments are prominent. Interestingly early occipital involvement in addition to striatal atrophy has also been reported for premanifest HD in the large-scale and longitudinal TRACK-HD study (Tabrizi et al., 2012). An important observation of TRACK-HD is that despite significant declines in brain volumes, only few functional measures showed longitudinal deterioration in premanifest HD (Tabrizi et al., 2012). This demonstrates that clinical manifestation does not simply depend on the extent of cell degeneration but rather represent a complex interaction within neuronal circuits, in which network reorganization or compensatory mechanisms may account for neuronal dysfunction to maintain functions. Our data clearly emphasizes that the assessment of any relationship between brain structure and behavior needs to consider the functional circuits formed by these anatomical regions. In other words, the predictive value of early structural alterations in HD for potential cognitive disturbances may be increased when functional networks formed by these alterations are taken into account. The here delineated cortico-striatal map associated with cognitive functioning may serve as a framework for future studies assessing potential network alterations in the context of behavior changes and monitoring disease progression in premanifest HD.

4.2. Functional connectivity of atrophy seeds in the manifest HD stage

Functional connectivity modeling of early manifest cortico-striatal seeds revealed two partly overlapping but functionally segregated networks that were driven by distinct behavioral tasks. According to the proposed basal ganglia-thalamo-cortical circuits (Alexander et al., 1986; Draganski et al., 2008), the dorsolateral prefrontal cognitive loop connects the caudate with the frontal and parietal cortices, while the motor loop connects the putamen with the motor and sensorimotor areas (i.e., PMC, SMA, M1, SI).

In accordance with this, in our connectivity modeling approach based on morphometric changes in manifest HD, M1-striatal seeds showed common functional connectivity with the putamen, pallidum, thalamus, posterior insula, Broca's area, premotor and sensorimotor cortices and inferior parietal regions. These seeds were also functionally associated with movement or action related tasks. Remarkably, HD manifests with a wide range of motor impairment extending beyond chorea (e.g., bradykinesia, rigidity, dystonia, dysphagia, dysarthria) and changing over time. This motor-related phenotypic heterogeneity is explained via dysfunctions of neurons within different (direct and indirect) motor control pathways linking the cortex with the basal ganglia (Albin et al., 1989). Importantly, additional cortical damage (either primary or secondary to striatal loss), such as atrophy in M1 as shown in our analysis, may further account for the complexity of HD's motor profile *via* widespread disruptions among motor areas and other cortices. In particular, the posterior insula, part of both our MACM and resting-state M1-striatal maps, is connected to the primary and secondary somatosensory and motor areas, and activated by sensorimotor tasks (Kurth et al., 2010b). The IPC is associated with multisensory integration and sensorimotor adaptation, and plays an important role within the motor system (Mattingley et al., 1998; Rozzi et al., 2008). Although HD-specific impairments of voluntary movement control are often ascribed to striatal degeneration, motor pathways and sensorimotor cortices are known to be selectively vulnerable in HD (Bohanna et al., 2011a; Rosas et al., 2008), and there is evidence of cortical contribution to HD's phenotype beyond striatal connectivity (Rosas et al., 2008). Also, within our ALE meta-data (Dogan et al., 2013) correlation analysis of convergent atrophy with UHDRS motor scores primarily yielded significant associations with cortical sensorimotor and premotor areas underlying motor functioning rather than with the striatum. Therefore and particularly when striatal loss has already progressed to differentiate within clinical profiles, the here delineated motor network derived from the connectivity modeling of striatal as well as cortical atrophy complements an ample understanding of striato–thalamo-cortical circuits early affected by HD's neuropathology.

Functional connectivity modeling of IFJ-striatal seeds revealed a rather cognitive network similar to the one observed using premanifest seeds, though more extensive both subcortically and cortically, and additionally including the thalamic nuclei connecting to the prefrontal and temporal cortices, as well as the medial prefrontal and cingulate areas. Behavioral characterization showed attention, working memory and language related cognitive domains, which are known to be more severely impaired in the manifest stage of HD (Paulsen, 2011). Hence, the delineated cognitive co-activation profile can be regarded as a possible neural network underlying such impairments in affected HD patients, although we cannot infer the specific pattern of activation within networks. In the IMAGE-HD study, Georgiou-Karistianis et al. (2013) reported increased task-based connectivity in manifest HD over 18 months in the left DLPFC and anterior cingulate connection, and decreased connectivity over time between the anterior cingulate and right caudate, which the authors interpreted as a change of neural response pattern possibly due to the extent of neuronal damage. While reduced interregional connectivity accords with DTI-based structural connectivity studies in HD (e.g., Bohanna et al., 2011b; Rosas et al., 2010), enhanced neural activation is often interpreted as compensatory recruitment representing primary dysfunctions with respect to cortical degeneration or secondary compensatory processes due to striatal deficits in HD (Georgiou-Karistianis, 2009; Paulsen, 2009). Once the neuronal loss progresses over time, these compensatory mechanisms may not be sustained to increase cognitive functioning (Georgiou-Karistianis

et al., 2013). This might explain the heterogeneous picture of decreased and increased functional connectivity in HD also reported in resting-state fMRI studies (Dumas et al., 2013; Poudel et al., 2014), where network alterations are more difficult to relate to specific behavior. However, in a recent resting-state study controlled for structural atrophy, we could demonstrate that increased intrinsic functional connectivity mainly in motor and parietal cortices was associated with motor impairment in HD patients (Werner et al., 2014).

Only few studies have addressed the impact of regional volume loss on functional connectivity in HD. Wolf et al. (2014) found increased intrinsic connectivity within striatal, motor and prefrontal resting-state networks, but also decreased connectivity within anterior and lateral prefrontal networks. After controlling for structural atrophy, observed alterations remained stable in the motor network, while some differences were not evident and others emerged after accounting for structural degeneration (Wolf et al., 2014). This indicates that functional connectivity changes may be explained or occur because of regional volume loss, or even can only be unveiled when brain volume is taken into account. Quarantelli et al. (2013) assessed DMN integrity and also demonstrated that connectivity changes in the caudate, SMA, insula and occipital cortex could be explained by regional atrophy, while other observed alterations in DMN nodes seemed to be unrelated to regional atrophy. Importantly, by partialling out differences in gray matter in functional imaging data (Oakes et al., 2007), the resulting connectivity patterns may not be directly attributed to or explained merely by the presence of overt volume loss. However, structural degeneration and in particular cortico-striatal atrophy massively impact cortico–striato–thalamo-cortical circuits which in turn may lead to disturbed functionality and mediate network connectivity. As argued above, an appropriate understanding of clinical manifestations in HD needs to consider both structural damage as well as the complex interactions between regions, since neural functionality is not conceivable without structural integrity or at least requires some sort of neural reorganization to maintain function. This implies that for the search of reliable biomarkers and in clinical trials designated to monitor disease progression and potential treatment effects, structural imaging methods should be accompanied by functional network analyses. However, in contrast to resting-state fMRI, task-based functional imaging may be problematic in advanced stages of HD due to patients' inability to comply with task performance. Therefore, the here proposed methods using MACM to assess task-dependent functional connectivity, behavioral decoding to characterize the associated functional role of networks, complemented by endogenously driven resting-state connectivity analyses offer a framework into brain-structure function investigations in HD. Combining these approaches will provide a more differentiated picture of cortical–subcortical disturbances emanating from HD-related structural degeneration and increase the predictive value of such alterations as reliable and clinically meaningful biomarkers in HD.

5. Limitations

Based on convergent structural alterations in HD, we were able to delineate functional networks co-activating with these regions, hence forming circuits that are potentially disrupted early in the disease. Albeit a pivotal role can be ascribed to these circuits in the pathophysiology of HD, the sequence of dysfunctions in these networks or the cumulative effect of gradual disease severity (e.g., genetic burden) on functional connectivity cannot be assessed from our data. Further, it is important to note that co-activation patterns derived from MACM or resting-state fMRI data include both direct and indirect connectivity between brain regions and do not imply any causality. Functional connectivity identifies brain regions that are synchronously co-activated and therefore reveals inter-regional relationships based on temporal fluctuations in fMRI BOLD response. This indirect method is highly complemented by structural analyses (e.g., DTI, fiber tracking) and the assessment of

de facto (direct or indirect) structural connections within functionally defined networks. Nonetheless, our multi-modal approach combines both (endogenously driven) task-free and (externally driven) task-based states of brain function allowing a complementary and robust delineation of functional connectivity (Eickhoff and Grefkes, 2011; Rottschy et al., 2013). While coactivation patterns revealed by MACM represent networks that are conjointly and consistently recruited across a broad range of experimental conditions, correlations of signal fluctuations in resting-state fMRI data provide insights into internally driven connectivity patterns. As stated above, we cannot make assumptions on the specific pattern of alterations within the proposed networks, whether there is increased or decreased coupling to be expected in HD patients. The outlined literature on functional connectivity in HD clearly shows divergent findings on this issue dependent on certain disease stages, which mirrors the heterogeneity of HD. Another drawback that is particularly relevant for our connectivity analysis of atrophy in the striatum is that we cannot determine the differential aspects of striatal connectivity since convergent clusters of striatal atrophy were large yielding a widespread network of task-based and resting-state connectivity. Our aim was to functionally characterize the functional networks formed by both striatal as well as cortical atrophic areas prominent in HD in order to unveil networks highly exposed to disease-related disruptions. Other meta-analytic techniques, such as connectivity-based parcellation (Bzdok et al., 2013; Eickhoff et al., 2011; Fox et al., 2014), are more suited to detect distinct patterns of functional connectivity within HD-related striatal atrophy, adding to a more differentiated picture of early cortico-striatal alterations in HD.

6. Summary and conclusions

We utilized both task-based MACM and resting-state connectivity data as powerful methods to investigate the functional and ensuing clinical relevance of structural damage in HD, providing an important link between morphometrically defined seed-regions and corresponding functional circuits. Our multi-modal approach delineated a segregation of a cognitive and a motor cortico-striatal loop in different stages of the disease. In premanifest HD, cortico-striatal atrophy seeds showed common co-activation with a rather cognitive network including the dorsal caudate nucleus, anterior insula, and lateral prefrontal, premotor and parietal regions, that was also driven by cognitive tasks such as working memory, reasoning and reward tasks. Combining both task-based and resting-state network analysis, our findings suggest that the DLPFC seems to be a core region prone to network alterations in the premanifest stage of HD. Functional connectivity modeling of early manifest cortico-striatal seeds revealed two partly overlapping but functionally segregated networks that were driven by distinct behavioral tasks. The co-activation pattern of IFJ-striatal seeds revealed a similar rather cognitive network, but more extensive both in task-driven and resting-state connectivity, including the dorsal caudate nucleus, ventral putamen, anterior insula, prefrontal cortex and premotor and supplementary motor areas. Functional attribution indicated involvement of this network in attention, working memory and language related cognitive domains known to be impaired in early manifest HD. In contrast M1-striatal atrophy seeds were driven by motor related tasks and forming a motor loop mainly consisting of the putamen, thalamus, posterior insula, and premotor and sensorimotor cortices. Overall, these outlined functional connectivity maps demonstrate a neurobiological basis for cognition-related disturbances in the premanifest stage of HD, as well as for cognitive behavioral features and the motor disorder after clinical conversion. These functional circuits may provide hypotheses for future studies and targeted experiments and potentially offer a framework in monitoring network alterations in HD.

Conflicts of interest

The authors declare that they have no conflict of interest.

Acknowledgments

Appendix A. Supplementary data

Supplementary material for this article can be found online at http://dx.doi.org/10.1016/j.nicl.2015.02.018.

References

Albin, R.L., Young, A.B., Penney, J.B., 1989. The functional anatomy of basal ganglia disorders. Trends Neurosci. 12 (10), 366–375. http://dx.doi.org/10.1016/0166-2236(89)90074-X2479133.

Alexander, G.E., DeLong, M.R., Strick, P.L., 1986. Parallel organization of functionally segregated circuits linking basal ganglia and cortex. Annu. Rev. Neurosci. 9, 357–381. http://dx.doi.org/10.1146/annurev.ne.09.030186.0020413085570.

Amunts, K., Kedo, O., Kindler, M., Pieperhoff, P., Mohlberg, H., Shah, N.J., Habel, U., Schneider, F., Zilles, K., 2005. Cytoarchitectonic mapping of the human amygdala, hippocampal region and entorhinal cortex: intersubject variability and probability maps. Anat. Embryol. 210 (5–6), 343–352. http://dx.doi.org/10.1007/s00429-005-0025-516208455.

Amunts, K., Schleicher, A., Bürgel, U., Mohlberg, H., Uylings, H.B., Zilles, K., 1999. Broca's region revisited: cytoarchitecture and intersubject variability. J. Comp. Neurol. 412 (2), 319–341. http://dx.doi.org/10.1002/(SICI)1096-9861(19990920)412:2<319::AID-CNE10>3.0.CO;2-710441759.

Ashburner, J., Friston, K.J., 2005. Unified segmentation. Neuroimage 26 (3), 839–851. http://dx.doi.org/10.1016/j.neuroimage.2005.02.01815955494.

Aylward, E.H., Nopoulos, P.C., Ross, C.A., Langbehn, D.R., Pierson, R.K., Mills, J.A., Johnson, H.J., Magnotta, V.A., Juhl, A.R., Paulsen, J.S., PREDICT-HD Investigators and Coordinators of Huntington Study Group, 2011. Longitudinal change in regional brain volumes in prodromal Huntington disease. J. Neurol. Neurosurg. Psychiatry 82, 405–410. http://dx.doi.org/10.1136/jnnp.2010.20826420884680.

Aylward, E.H., Sparks, B.F., Field, K.M., Yallapragada, V., Shpritz, B.D., Rosenblatt, A., Brandt, J., Gourley, L.M., Liang, K., Zhou, H., et al., 2004. Onset and rate of striatal atrophy in preclinical Huntington disease. Neurology 63 (1), 66–72. http://dx.doi.org/10.1212/01.WNL.0000132965.14653.D115249612.

Behrens, T.E., Johansen-Berg, H., Woolrich, M.W., Smith, S.M., Wheeler-Kingshott, C.A., Boulby, P.A., Barker, G.J., Sillery, E.L., Sheehan, K., Ciccarelli, O., et al., 2003. Non-invasive mapping of connections between human thalamus and cortex using diffusion imaging. Nat. Neurosci. 6 (7), 750–757. http://dx.doi.org/10.1038/nn107512808459.

Biswal, B., Yetkin, F.Z., Haughton, V.M., Hyde, J.S., 1995. Functional connectivity in the motor cortex of resting human brain using echo-planar MRI. Magn. Reson. Med. 34 (4), 537–541. http://dx.doi.org/10.1002/mrm.19103404098524021.

Bohanna, I., Georgiou-Karistianis, N., Egan, G.F., 2011a. Connectivity-based segmentation of the striatum in Huntington's disease: vulnerability of motor pathways. Neurobiol. Dis. 42 (3), 475–481. http://dx.doi.org/10.1016/j.nbd.2011.02.01021382492.

Bohanna, I., Georgiou-Karistianis, N., Sritharan, A., Asadi, H., Johnston, L., Churchyard, A., Egan, G., 2011b. Diffusion tensor imaging in Huntington's disease reveals distinct patterns of white matter degeneration associated with motor and cognitive deficits. Brain Imaging Behav. 5 (3), 171–180. http://dx.doi.org/10.1007/s11682-011-9121-821437574.

Bzdok, D., Laird, A.R., Zilles, K., Fox, P.T., Eickhoff, S.B., 2013. An investigation of the structural, connectional, and functional subspecialization in the human amygdala. Hum. Brain Mapp. 34 (12), 3247–3266. http://dx.doi.org/10.1002/hbm.2213822806915.

Caspers, S., Eickhoff, S.B., Geyer, S., Scheperjans, F., Mohlberg, H., Zilles, K., Amunts, K., 2008. The human inferior parietal lobule in stereotaxic space. Brain Struct. Funct. 212 (6), 481–495. http://dx.doi.org/10.1007/s00429-008-0195-z18651173.

Choi, H.J., Zilles, K., Mohlberg, H., Schleicher, A., Fink, G.R., Armstrong, E., Amunts, K., 2006. Cytoarchitectonic identification and probabilistic mapping of two distinct areas within the anterior ventral bank of the human intraparietal sulcus. J. Comp. Neurol. 495 (1), 53–69. http://dx.doi.org/10.1002/cne.2084916432904.

Clos, M., Amunts, K., Laird, A.R., Fox, P.T., Eickhoff, S.B., 2013. Tackling the multifunctional nature of Broca's region meta-analytically: co-activation-based parcellation of area 44. Neuroimage 83, 174–188. http://dx.doi.org/10.1016/j.neuroimage.2013.06.04123791915.

Diedrichsen, J., Balsters, J.H., Flavell, J., Cussans, E., Ramnani, N., 2009. A probabilistic MR atlas of the human cerebellum. Neuroimage 46 (1), 39–46. http://dx.doi.org/10.1016/j.neuroimage.2009.01.04519457380.

Dogan, I., Eickhoff, S.B., Schulz, J.B., Shah, N.J., Laird, A.R., Fox, P.T., Reetz, K., 2013. Consistent neurodegeneration and its association with clinical progression in Huntington's disease: a coordinate-based meta-analysis. Neurodegener. Dis. 12 (1), 23–35. http://dx.doi.org/10.1159/00033952822922585.

Dogan, I., Saß, C., Mirzazade, S., Kleiman, A., Werner, C.J., Pohl, A., Schiefer, J., Binkofski, F., Schulz, J.B., Shah, N.J., et al., 2014. Neural correlates of impaired emotion processing in

manifest Huntington's disease. Soc. Cogn. Affect. Neurosci. 9 (5), 671–680. http://dx.doi.org/10.1093/scan/nst02923482620.

Draganski, B., Kherif, F., Klöppel, S., Cook, P.A., Alexander, D.C., Parker, G.J., Deichmann, R., Ashburner, J., Frackowiak, R.S., 2008. Evidence for segregated and integrative connectivity patterns in the human basal ganglia. J. Neurosci. 28 (28), 7143–7152. http://dx.doi.org/10.1523/JNEUROSCI.1486-08.200818614684.

Dumas, E.M., van den Bogaard, S.J., Hart, E.P., Soeter, R.P., van Buchem, M.A., van der Grond, J., Rombouts, S.A., Roos, R.A., TRACK-HD Investigator Group, 2013. Reduced functional brain connectivity prior to and after disease onset in Huntington's disease. Neuroimage Clin. 2, 377–384. http://dx.doi.org/10.1016/j.nicl.2013.03.00124179791.

Eickhoff, S.B., Bzdok, D., Laird, A.R., Kurth, F., Fox, P.T., 2012. Activation likelihood estimation meta-analysis revisited. Neuroimage 59 (3), 2349–2361. http://dx.doi.org/10.1016/j.neuroimage.2011.09.01721963913.

Eickhoff, S.B., Bzdok, D., Laird, A.R., Roski, C., Caspers, S., Zilles, K., Fox, P.T., 2011. Co-activation patterns distinguish cortical modules, their connectivity and functional differentiation. Neuroimage 57 (3), 938–949. http://dx.doi.org/10.1016/j.neuroimage.2011.05.02121609770.

Eickhoff, S.B., Grefkes, C., 2011. Approaches for the integrated analysis of structure, function and connectivity of the human brain. Clin. E.E.G. Neurosci. 42 (2), 107–121. http://dx.doi.org/10.1177/15500594110420021121675600.

Eickhoff, S.B., Jbabdi, S., Caspers, S., Laird, A.R., Fox, P.T., Zilles, K., Behrens, T.E., 2010. Anatomical and functional connectivity of cytoarchitectonic areas within the human parietal operculum. J. Neurosci. 30 (18), 6409–6421. http://dx.doi.org/10.1523/JNEUROSCI.5664-09.201020445067.

Eickhoff, S.B., Laird, A.R., Grefkes, C., Wang, L.E., Zilles, K., Fox, P.T., 2009. Coordinate-based activation likelihood estimation meta-analysis of neuroimaging data: a random-effects approach based on empirical estimates of spatial uncertainty. Hum. Brain Mapp. 30 (9), 2907–2926. http://dx.doi.org/10.1002/hbm.2071819172646.

Eickhoff, S.B., Paus, T., Caspers, S., Grosbras, M.H., Evans, A.C., Zilles, K., Amunts, K., 2007. Assignment of functional activations to probabilistic cytoarchitectonic areas revisited. Neuroimage 36 (3), 511–521. http://dx.doi.org/10.1016/j.neuroimage.2007.03.06017499520.

Eickhoff, S.B., Schleicher, A., Zilles, K., Amunts, K., 2006. The human parietal operculum. I. Cytoarchitectonic mapping of subdivisions. Cereb. Cortex 16 (2), 254–267. http://dx.doi.org/10.1093/cercor/bhi10515888607.

Eickhoff, S.B., Stephan, K.E., Mohlberg, H., Grefkes, C., Fink, G.R., Amunts, K., Zilles, K., 2005. A new SPM toolbox for combining probabilistic cytoarchitectonic maps and functional imaging data. Neuroimage 25 (4), 1325–1335. http://dx.doi.org/10.1016/j.neuroimage.2004.12.03415850749.

Fox, M.D., Raichle, M.E., 2007. Spontaneous fluctuations in brain activity observed with functional magnetic resonance imaging. Nat. Rev. Neurosci. 8 (9), 700–711. http://dx.doi.org/10.1038/nrn220117704812.

Fox, P.T., Lancaster, J.L., Laird, A.R., Eickhoff, S.B., 2014. Meta-analysis in human neuroimaging: computational modeling of large-scale databases. Annu. Rev. Neurosci. 37, 409–434. http://dx.doi.org/10.1146/annurev-neuro-062012-17032025032500.

Georgiou-Karistianis, N., 2009. A peek inside the Huntington's brain: will functional imaging take us one step closer in solving the puzzle? Exp. Neurol. 220 (1), 5–8. http://dx.doi.org/10.1016/j.expneurol.2009.08.00119679124.

Georgiou-Karistianis, N., Poudel, G.R., Dominguez, D.J., Langmaid, R., Gray, M.A., Churchyard, A., Chua, P., Borowsky, B., Egan, G.F., Stout, J.C., 2013. Functional and connectivity changes during working memory in Huntington's disease: 18 month longitudinal data from the IMAGE-HD study. Brain Cogn. 83 (1), 80–91. http://dx.doi.org/10.1016/j.bandc.2013.07.00423938592.

Geyer, S., 2004. The microstructural border between the motor and the cognitive domain in the human cerebral cortex. Adv. Anat. Embryol. Cell Biol. 174, I–VIII14750415.

Geyer, S., Ledberg, A., Schleicher, A., Kinomura, S., Schormann, T., Bürgel, U., Klingberg, T., Larsson, J., Zilles, K., Roland, P.E., 1996. Two different areas within the primary motor cortex of man. Nature 382 (6594), 805–807. http://dx.doi.org/10.1038/382805a08752272.

Geyer, S., Schleicher, A., Zilles, K., 1999. Areas 3a, 3b, and 1 of human primary somatosensory cortex. Neuroimage 10 (1), 63–83. http://dx.doi.org/10.1006/nimg.1999.044010385582.

Geyer, S., Schormann, T., Mohlberg, H., Zilles, K., 2000. Areas 3a, 3b, and 1 of human primary somatosensory cortex. Part 2. Spatial normalization to standard anatomical space. Neuroimage 11 (6 1), 684–696. http://dx.doi.org/10.1006/nimg.2000.054810860796.

Henley, S.M., Wild, E.J., Hobbs, N.Z., Warren, J.D., Frost, C., Scahill, R.I., Ridgway, G.R., MacManus, D.G., Barker, R.A., Fox, N.C., et al., 2008. Defective emotion recognition in early HD is neuropsychologically and anatomically generic. Neuropsychologia 46 (8), 2152–2160. http://dx.doi.org/10.1016/j.neuropsychologia.2008.02.02518407301.

Hennenlotter, A., Schroeder, U., Erhard, P., Haslinger, B., Stahl, R., Weindl, A., von Einsiedel, H.G., Lange, K.W., Ceballos-Baumann, A.O., 2004. Neural correlates associated with impaired disgust processing in pre-symptomatic Huntington's disease. Brain 127 (6), 1446–1453. http://dx.doi.org/10.1093/brain/awh1615090475.

Kurth, F., Eickhoff, S.B., Schleicher, A., Hoemke, L., Zilles, K., Amunts, K., 2010a. Cytoarchitecture and probabilistic maps of the human posterior insular cortex. Cereb. Cortex 20 (6), 1448–1461. http://dx.doi.org/10.1093/cercor/bhp20819822572.

Kurth, F., Zilles, K., Fox, P.T., Laird, A.R., Eickhoff, S.B., 2010b. A link between the systems: functional differentiation and integration within the human insula revealed by meta-analysis. Brain Struct. Funct. 214 (5–6), 519–534. http://dx.doi.org/10.1007/s00429-010-0255-z.

Laird, A.R., Eickhoff, S.B., Fox, P.M., Uecker, A.M., Ray, K.L., Saenz Jr., J.J., McKay, D.R., Bzdok, D., Laird, R.W., Robinson, J.L., et al., 2011. The BrainMap strategy for standardization, sharing, and meta-analysis of neuroimaging data. B.M.C. Res. Notes 4, 349. http://dx.doi.org/10.1186/1756-0500-4-34921906305.

Laird, A.R., Eickhoff, S.B., Kurth, F., Fox, P.M., Uecker, A.M., Turner, J.A., Robinson, J.L., Lancaster, J.L., Fox, P.T., 2009a. ALE meta-analysis workflows via the BrainMap

database: progress towards a probabilistic functional brain atlas. Front. Neuroinformatics 3, 23. http://dx.doi.org/10.3389/neuro.11.023.200919636392.

Laird, A.R., Eickhoff, S.B., Li, K., Robin, D.A., Glahn, D.C., Fox, P.T., 2009b. Investigating the functional heterogeneity of the default mode network using coordinate-based meta-analytic modeling. J. Neurosci. 29 (46), 14496–14505. http://dx.doi.org/10.1523/JNEUROSCI.4004-09.200919923283.

Mattingley, J.B., Husain, M., Rorden, C., Kennard, C., Driver, J., 1998. Motor role of human inferior parietal lobe revealed in unilateral neglect patients. Nature 392 (6672), 179–182. http://dx.doi.org/10.1038/324139515962.

Nichols, T., Brett, M., Andersson, J., Wager, T., Poline, J.B., 2005. Valid conjunction inference with the minimum statistic. Neuroimage 25 (3), 653–660. http://dx.doi.org/10.1016/j.neuroimage.2004.12.00515808966.

Nooner, K.B., Colcombe, S.J., Tobe, R.H., Mennes, M., Benedict, M.M., Moreno, A.L., Panek, L.J., Brown, S., Zavitz, S.T., Li, Q., et al., 2012. The NKI-Rockland sample: a model for accelerating the pace of discovery science in psychiatry. Front. Neurosci. 6, 152. http://dx.doi.org/10.3389/fnins.2012.0015223087608.

Novak, M.J., Warren, J.D., Henley, S.M., Draganski, B., Frackowiak, R.S., Tabrizi, S.J., 2012. Altered brain mechanisms of emotion processing in pre-manifest Huntington's disease. Brain 135 (4), 1165–1179. http://dx.doi.org/10.1093/brain/aws02422505631.

Oakes, T.R., Fox, A.S., Johnstone, T., Chung, M.K., Kalin, N., Davidson, R.J., 2007. Integrating VBM into the general linear model with voxelwise anatomical covariates. Neuroimage 34 (2), 500–508. http://dx.doi.org/10.1016/j.neuroimage.2006.10.00717113790.

Papp, K.V., Kaplan, R.F., Snyder, P.J., 2011. Biological markers of cognition in prodromal Huntington's disease: a review. Brain Cogn. 77 (2), 280–291. http://dx.doi.org/10.1016/j.bandc.2011.07.00921889251.

Paulsen, J.S., 2009. Functional imaging in Huntington's disease. Exp. Neurol. 216 (2), 272–277. http://dx.doi.org/10.1016/j.expneurol.2008.12.01519171138.

Paulsen, J.S., 2011. Cognitive impairment in Huntington disease: diagnosis and treatment. Curr. Neurol. Neurosci. Rep. 11 (5), 474–483. http://dx.doi.org/10.1007/s11910-011-0215-x21861097.

Paulsen, J.S., Hayden, M., Stout, J.C., Langbehn, D.R., Aylward, E., Ross, C.A., Guttman, M., Nance, M., Kieburtz, K., Oakes, D., et al., 2006. Preparing for preventive clinical trials: the Predict-HD study. Arch. Neurol. 63 (6), 883–890. http://dx.doi.org/10.1001/archneur.63.6.88316769871.

Paulsen, J.S., Nopoulos, P.C., Aylward, E., Ross, C.A., Johnson, H., Magnotta, V.A., Juhl, A., Pierson, R.K., Mills, J., Langbehn, D., et al., 2010. Striatal and white matter predictors of estimated diagnosis for Huntington disease. Brain Res. Bull. 82 (3–4), 201–207. http://dx.doi.org/10.1016/j.brainresbull.2010.04.00320385209.

Poudel, G.R., Egan, G.F., Churchyard, A., Chua, P., Stout, J.C., Georgiou-Karistianis, N., 2014. Abnormal synchrony of resting state networks in premanifest and symptomatic Huntington disease: the IMAGE-HD study. J. Psychiatry Neurosci. 39 (2), 87–9624083458.

Poudel, G.R., Stout, J.C., Domínguez, D.J., Gray, M.A., Salmon, L., Churchyard, A., Chua, P., Borowsky, B., Egan, G.F., Georgiou-Karistianis, N., 2015. Functional changes during working memory in Huntington's disease: 30-month longitudinal data from the IMAGE-HD study. Brain Struct. Funct. 220, 501–512. http://dx.doi.org/10.1007/s00429-013-0670-z24240602.

Quarantelli, M., Salvatore, E., Giorgio, S.M., Filla, A., Cervo, A., Russo, C.V., Cocozza, S., Massarelli, M., Brunetti, A., De Michele, G., 2013. Default-mode network changes in Huntington's disease: an integrated MRI study of functional connectivity and morphometry. PLOS One 8 (8), e72159. http://dx.doi.org/10.1371/journal.pone.007215923977239.

Reetz, K., Dogan, I., Rolfs, A., Binkofski, F., Schulz, J.B., Laird, A.R., Fox, P.T., Eickhoff, S.B., 2012. Investigating function and connectivity of morphometric findings — exemplified on cerebellar atrophy in spinocerebellar ataxia 17 (SCA17). Neuroimage 62 (3), 1354–1366. http://dx.doi.org/10.1016/j.neuroimage.2012.05.05822659444.

Rosas, H.D., Lee, S.Y., Bender, A.C., Zaleta, A.K., Vangel, M., Yu, P., Fischl, B., Pappu, V., Onorato, C., Cha, J.H., et al., 2010. Altered white matter microstructure in the corpus callosum in Huntington's disease: implications for cortical "disconnection". Neuroimage 49 (4), 2995–3004. http://dx.doi.org/10.1016/j.neuroimage.2009.10.01519850138.

Rosas, H.D., Salat, D.H., Lee, S.Y., Zaleta, A.K., Pappu, V., Fischl, B., Greve, D., Hevelone, N., Hersch, S.M., 2008. Cerebral cortex and the clinical expression of Huntington's disease: complexity and heterogeneity. Brain 131 (4), 1057–1068. http://dx.doi.org/10.1093/brain/awn02518337273.

Rottschy, C., Caspers, S., Roski, C., Reetz, K., Dogan, I., Schulz, J.B., Zilles, K., Laird, A.R., Fox, P.T., Eickhoff, S.B., 2013. Differentiated parietal connectivity of frontal regions for "what" and "where" memory. Brain Struct. Funct. 218, 1551–1567. http://dx.doi.org/10.1007/s00429-012-0476-423143344.

Rozzi, S., Ferrari, P.F., Bonini, L., Rizzolatti, G., Fogassi, L., 2008. Functional organization of inferior parietal lobule convexity in the macaque monkey: electrophysiological characterization of motor, sensory and mirror responses and their correlation with cytoarchitectonic areas. Eur. J. Neurosci. 28 (8), 1569–1588. http://dx.doi.org/10.1111/j.1460-9568.2008.06395.x18691325.

Scheperjans, F., Hermann, K., Eickhoff, S.B., Amunts, K., Schleicher, A., Zilles, K., 2008. Observer-independent cytoarchitectonic mapping of the human superior parietal cortex. Cereb. Cortex 18 (4), 846–867. http://dx.doi.org/10.1093/cercor/bhm11617644831.

Schmahmann, J.D., 1991. An emerging concept. The cerebellar contribution to higher function. Arch. Neurol. 48 (11), 1178–1187. http://dx.doi.org/10.1001/archneur.1991.00530200860291953406.

Stout, J.C., Paulsen, J.S., Queller, S., Solomon, A.C., Whitlock, K.B., Campbell, J.C., Carlozzi, N., Duff, K., Beglinger, L.J., Langbehn, D.R., et al., 2011. Neurocognitive signs in prodromal Huntington disease. Neuropsychol. 25 (1), 1–14. http://dx.doi.org/10.1037/a002093720919768.

Tabrizi, S.J., Langbehn, D.R., Leavitt, B.R., Roos, R.A., Durr, A., Craufurd, D., Kennard, C., Hicks, S.L., Fox, N.C., Scahill, R.I., et al., 2009. Biological and clinical manifestations of Huntington's disease in the longitudinal TRACK-HD study: cross-sectional analysis of baseline data. Lancet Neurol. 8 (9), 791–801. http://dx.doi.org/10.1016/S1474-4422(09)70170-X19646924.

Tabrizi, S.J., Reilmann, R., Roos, R.A., Durr, A., Leavitt, B., Owen, G., Jones, R., Johnson, H., Craufurd, D., Hicks, S.L., et al., 2012. Potential endpoints for clinical trials in premanifest and early Huntington's disease in the TRACK-HD study: analysis of 24 month observational data. Lancet Neurol. 11 (1), 42–53. http://dx.doi.org/10.1016/S1474-4422(11)70263-022137354.

Tabrizi, S.J., Scahill, R.I., Durr, A., Roos, R.A., Leavitt, B.R., Jones, R., Landwehrmeyer, G.B., Fox, N.C., Johnson, H., Hicks, S.L., et al., 2011. Biological and clinical changes in premanifest and early stage Huntington's disease in the TRACK-HD study: the 12-month longitudinal analysis. Lancet Neurol. 10 (1), 31–42. http://dx.doi.org/10.1016/S1474-4422(10)70276-321130037.

Tabrizi, S.J., Scahill, R.I., Owen, G., Durr, A., Leavitt, B.R., Roos, R.A., Borowsky, B., Landwehrmeyer, B., Frost, C., Johnson, H., et al., 2013. Predictors of phenotypic progression and disease onset in premanifest and early-stage Huntington's disease in the TRACK-HD study: analysis of 36-month observational data. Lancet Neurol. 12 (7), 637–649. http://dx.doi.org/10.1016/S1474-4422(13)70088-723664844.

Turkeltaub, P.E., Eden, G.F., Jones, K.M., Zeffiro, T.A., 2002. Meta-analysis of the functional neuroanatomy of single-word reading: method and validation. Neuroimage 16 (3 1), 765–780. http://dx.doi.org/10.1006/nimg.2002.113112169260.

Turkeltaub, P.E., Eickhoff, S.B., Laird, A.R., Fox, M., Wiener, M., Fox, P., 2012. Minimizing within-experiment and within-group effects in activation likelihood estimation meta-analyses. Hum. Brain Mapp. 33 (1), 1–13. http://dx.doi.org/10.1002/hbm.2118621305667.

Unschuld, P.G., Joel, S.E., Liu, X., Shanahan, M., Margolis, R.L., Biglan, K.M., Bassett, S.S., Schretlen, D.J., Redgrave, G.W., van Zijl, P.C., et al., 2012. Impaired cortico-striatal functional connectivity in prodromal Huntington's disease. Neurosci. Lett. 514 (2), 204–209. http://dx.doi.org/10.1016/j.neulet.2012.02.09522425717.

Wager, T.D., Lindquist, M.A., Nichols, T.E., Kober, H., Van Snellenberg, J.X., 2009. Evaluating the consistency and specificity of neuroimaging data using meta-analysis. Neuroimage 45, S210–21.

Werner, C.J., Dogan, I., Saß, C., Mirzazade, S., Schiefer, J., Shah, N.J., Schulz, J.B., Reetz, K., 2014. Altered resting-state connectivity in Huntington's disease. Hum. Brain Mapp. 35 (6), 2582–2593. http://dx.doi.org/10.1002/hbm.2235123982979.

Wolf, R.C., Klöppel, S., 2013. Clinical significance of frontal cortex abnormalities in Huntington's disease. Exp. Neurol. 247, 39–44. http://dx.doi.org/10.1016/j.expneurol.2013.03.02223562669.

Wolf, R.C., Sambataro, F., Vasic, N., Depping, M.S., Thomann, P.A., Landwehrmeyer, G.B., Süssmuth, S.D., Orth, M., 2014. Abnormal resting-state connectivity of motor and cognitive networks in early manifest Huntington's disease. Psychol. Med. 44, 3341–3356. http://dx.doi.org/10.1017/S003329171400057925066491.

Wolf, R.C., Sambataro, F., Vasic, N., Schönfeldt-Lecuona, C., Ecker, D., Landwehrmeyer, B., 2008a. Altered frontostriatal coupling in pre-manifest Huntington's disease: effects of increasing cognitive load. Eur. J. Neurol. 15 (11), 1180–1190. http://dx.doi.org/10.1111/j.1468-1331.2008.02253.x18754766.

Wolf, R.C., Sambataro, F., Vasic, N., Schönfeldt-Lecuona, C., Ecker, D., Landwehrmeyer, B., 2008b. Aberrant connectivity of lateral prefrontal networks in presymptomatic Huntington's disease. Exp. Neurol. 213 (1), 137–144. http://dx.doi.org/10.1016/j.expneurol.2008.05.01718588876.

Wolf, R.C., Vasic, N., Schönfeldt-Lecuona, C., Ecker, D., Landwehrmeyer, G.B., 2009. Cortical dysfunction in patients with Huntington's disease during working memory performance. Hum. Brain Mapp. 30 (1), 327–339. http://dx.doi.org/10.1002/hbm.2050218172852.

Wolf, R.C., Vasic, N., Schönfeldt-Lecuona, C., Landwehrmeyer, G.B., Ecker, D., 2007. Dorsolateral prefrontal cortex dysfunction in presymptomatic Huntington's disease: evidence from event-related fMRI. Brain 130 (11), 2845–2857. http://dx.doi.org/10.1093/brain/awm21017855375.

Zu Eulenburg, P., Caspers, S., Roski, C., Eickhoff, S.B., 2012. Meta-analytical definition and functional connectivity of the human vestibular cortex. Neuroimage 60 (2012), 162–169.